Chapter 20
Image Analysis for Oleogel and Oleogel-Based System Characterization

Camila Palla and Fabio Valoppi

Abbreviations

AFM	Atomic force microscopy
CLSM	Confocal scanning laser microscopy
CRM	Confocal Raman microscopy
Cryo-SEM	Cryogenic scanning electron microscopy
Cryo-TEM	Cryogenic transmission electron microscopy
CTI	X-ray computed tomography imaging
D	Fractal dimension
DIP	Digital image processing
FFT	Fast Fourier transform

Camila Palla and Fabio Valoppi contributed equally

C. Palla (✉)
Departamento de Ingeniería Química, Universidad Nacional del Sur (UNS), Bahía Blanca, Argentina

Planta Piloto de Ingeniería Química - PLAPIQUI (UNS-CONICET), Bahía Blanca, Argentina
e-mail: cpalla@plapiqui.edu.ar

F. Valoppi
Electronics Research Laboratory, Department of Physics, University of Helsinki, Helsinki, Finland

Department of Food and Nutrition, University of Helsinki, Helsinki, Finland

Helsinki Institute of Sustainability Science, Faculty of Agriculture and Forestry, University of Helsinki, Helsinki, Finland

Helsinki Institute of Life Science, University of Helsinki, Helsinki, Finland
e-mail: fabio.valoppi@helsinki.fi

C. Andrea Palla, F. Valoppi (eds.), *Advances in Oleogel Development, Characterization, and Nutritional Aspects*,
https://doi.org/10.1007/978-3-031-46831-5_20

MG	Monoglyceride
ML	Machine learning
MRI	Magnetic resonance imaging
PAF	Pore area fraction
PLM	Polarized light microscopy
RM	Rheo-microscope
SEM	Scanning electron microscopy
TEM	Transmission electron microscopy
UV	Ultraviolet
XRD	X-ray diffraction

20.1 Introduction

Imaging is a qualitative tool commonly employed to visually support numerical data. Besides giving tangible and concrete support to data, images contain embedded information that can be extracted and quantified using image analysis. Thus, image analysis can be a powerful tool able to enrich the pool of techniques available to characterize and explain material properties. In general, we can refer to image analysis as the set of actions needed to extract specific information from digital images. Data obtained through image analysis are then interpreted based on the equipment used to generate the original images. Usually, we can extract information about the structure and behavior of materials at macro-, micro-, and nanoscale. The type of information obtained is based on the intensity and distribution of pixels (in 2D images) or voxels (in 3D images), which are the smallest elements forming an image. Image analysis can be performed using freeware or licensed software. These programs often embed most of the necessary commands and plugins for image editing and processing, as well as the possibility to automate the process through macros and scripts.

In the field of oleogels, images are usually obtained through digital cameras, light microscopy (such as brightfield and polarized light), scanning or transmission electron microscopy (SEM or TEM), and their cryogenic versions (Cryo-SEM or Cryo-TEM). Other advanced or more recent imaging techniques applied to oleogels include magnetic resonance imagining, Raman microscopy, and atomic force microscopy. From these images, it is possible to calculate multiple parameters to characterize crystal/polymer networks in oleogels, as well as the spatial distribution of oleogels in food products when used as ingredients. When images are taken by varying time (during storage), temperature (during heating and cooling at defined rates), or shear (controlled deformation through the application of stress), we can determine the influence of such external forces/stimuli on oleogels and calculate—depending on the modified variable—kinetics of crystallization and network formation, polymorphic transformation, melting and network breakup, or oil release kinetics, to name a few. Thus, image analysis is not only useful for understanding the overall structure and behavior of oleogels but also for predicting their potential stability and applicability in real food products.

In this chapter, we summarize and explain the most common procedures and software used in the literature to analyze images of oleogels and similar lipid-based materials under static or dynamic conditions with the aim of obtaining relevant macro-, micro-, and nanostructural information. We have also included some examples of applications.

20.2 The Use of Image Analysis in Oleogel Characterization

20.2.1 Image Acquisition Techniques

Various imaging techniques have been used to acquire images of oleogels or oleogel-based systems, as shown in Table 20.1. Well-established 2D and 3D imaging techniques, commonly used for visualizing food microstructures, are mainly employed to capture and characterize micron and submicron-sized features of oleogels. Advanced imaging techniques are also employed to extract more specific information. In this section, we provide a brief overview of these techniques, their main characteristics, and their applications in the field of oleogels.

Optical (polarized light and brightfield) microscopy has been mainly adopted to qualitatively observe crystalline particles and their networks (Fig. 20.1a, b). A major advantage of optical microscopy is that it provides real-time, full-color images of samples in a non-destructive way [1]. Furthermore, by coupling a microscope with a stage that controls temperature, pressure, or shear, a variety of dynamic conditions can be applied to observe changes in the appearance of the sample. As an example, the rheo-microscope (RM) module allows optical images of internal structures of gels to be recorded simultaneously with rheological measurements, making it possible to visualize the effects of shear and deformation on sample structures.

Electron microscopy is used to image nanostructures and employ an electron beam instead of light which allows to increase the resolution limits from around 400–700 nm to 1–0.05 nm [2, 3]. Both scanning electron microscopy (SEM), which explores the surface topology of a sample, and transmission electron microscopy (TEM), which aims to visualize the internal structure of thinly sliced samples, have been used to analyze the morphological characteristics of oleogel networks (Fig. 20.1c, d). Cryogenic electron microscopy (Cryo-SEM and Cryo-TEM) is especially relevant for use with oleogel samples where the structure can be affected by high temperatures. With Cryo-SEM/TEM the fixation is performed by freezing the sample in an ultrafast cooling stage, protecting the material from direct damage from electron beam irradiation.

Confocal scanning laser microscopy (CSLM) uses a laser beam as a light source. A typical confocal microscope contains four laser lines covering the range from ultraviolet (UV) to infrared. The mode of operation involves focusing the light beam on small volumes, thereby imaging very fine focal planes that provide highly detailed optical sections through the sample [3, 4]. CSLM also allows multiple sections to be scanned at different depths to reconstruct a final 3D image of the

Table 20.1 Techniques used to capture images of oleogels, oleogel-based systems, and related lipid systems, along with the information extracted from image analysis

Technique	Measured features/analysis	System	References
Bright field microscopy	Crystal shape	Stearic acid/monoglyceride oleogels	[18]
	Crystal size	Wax and hydrolyzed wax oleogels	[19]
	Angles between crystal faces	Wax oleogels	[20]
	Bubble size kinetics	Wax-based oleofoam	[21]
Polarized light microscopy (PLM)	Crystal size Crystal size distribution Crystal shape Crystalline area/pore area Crystal fractal dimension	Wax oleogel Monoglyceride oleogel	[22] [23] [24]
Rheo-microscope	Crystal size Crystal size distribution Crystal shape Crystalline area/pore area Crystal fractal dimension Crystallization kinetics	Monoglyceride oleogel	[25] [23]
Scanning electron microscopy (SEM) and Cryo-SEM	Polymer network Pore diameter	Ethylcellulose oleogel	[6]
	Crystal shape	Fruit wax and lecithin oleogel	[26]
	Crystal network	Wax and hydrolyzed wax oleogels	[19]
Transmission electron microscopy (TEM) and Cryo-TEM	Crystal shape	Stearic acid/monoglyceride oleogels	[18]
	Lamellar dimension	Wax oleogel Wax oleogelsmonoglyceride Monoglyceride (MG)/stearic acid/ stearyl alcohol/ 2-hydroxyethyl stearate/octadecane oleogel	[27] [28]
Confocal laser scanning microscopy (CLSM)	Crystal size Crystal size distribution Crystal shape	Monoglyceride oleogel	[23]

	Crystalline area/pore area Crystal fractal dimension		
	Interfacial morphology	Beeswax oleogel-in-water Pickering emulsion	[29]
	Oleogel and hydrogel phase distribution	Bigel	[30]
Atomic force microscopy (AFM)	Polymer network Pore diameter Pore depth	Ethylcellulose oleogel	[6]
	Fibril shape Fibril growth mechanism	Sitosterol-oryzanol oleogel	[7]
Confocal Raman microscopy (CRM)	Size and porosity of fat crystal flocs Fractal dimension	Micronized fat crystals in oil	[10]
	Crystallinity index Polymorphic form identification	Porcine fat	[11]
	Microstructure Maps of component distribution	Ethylcellulose and anhydrous milk fat oleogel	[12]
	Stability against phase separation	Oleogel-based oleofoams	[5]
Magnetic resonance imaging (MRI)	Mobility of lipid protons	Sweet bread containing monoglyceride oleogel	[13]
X-ray computed tomography imaging (CTI)	Object volume Structure thickness Porosity	Oleogel-based filling cream	[15]
	Porosity	Oleogel-based muffins	[31]
Digital camera (macroscopic images)	Oil release kinetics	Monoglyceride oleogel	[17]
	Crumb grain features (air cells size and number)	Oleogel-based muffin	[16]

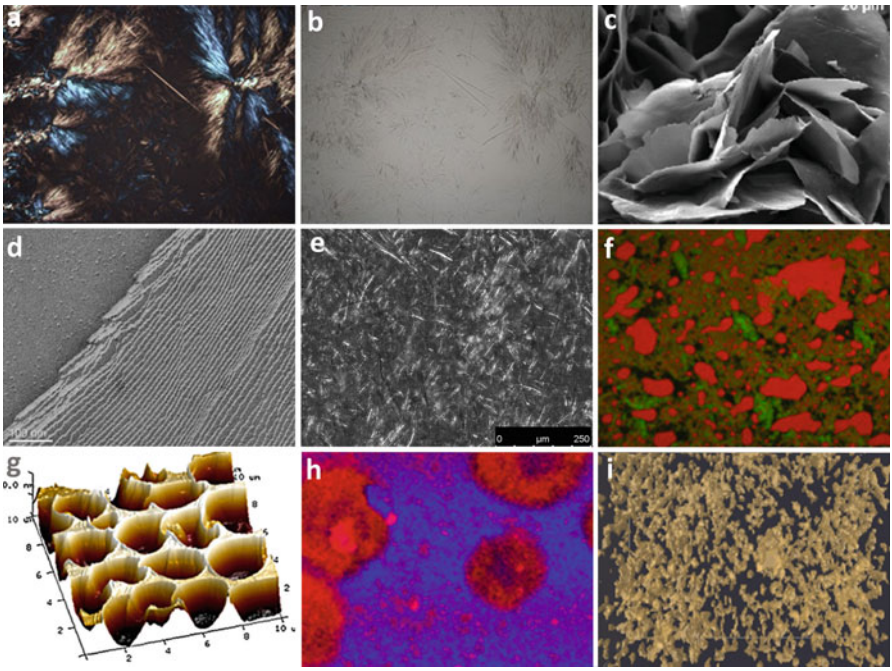

Fig. 20.1 Images acquired with different imagining techniques: (**a**) PLM, sample: monoglyceride (MG): phytosterol oleogel. (Reproduced from [32], with permission from John Wiley & Sons); (**b**) Brightfield microscopy, sample: MG: phytosterol oleogel. (Reproduced from [32], with permission from John Wiley & Sons); (**c**) Cryo-SEM, sample: sunflower wax oleogel. (Reproduced from [19], with permission from John Wiley & Sons, under the terms of the Creative Commons CC-BY-NC-ND 4.0 license); (**d**) TEM, sample: stearic acid oleogel. (Reproduced from [18], with permission from Elsevier); (**e**) CLSM, sample: MG oleogel; (**f**) CLSM, sample: 50:50 bigel (dyed hydrogel fluoresces green and dyed oleogel fluoresces red). (Reproduced from [30], with permission from Elsevier, under the terms of the Creative Commons CC-BY-NC-ND 4.0 license); (**g**) AFM, sample: ethylcellulose oleogel. (Reproduced from [6], with permission from Elsevier); (**h**) CRM, sample: ethylcellulose and anhydrous milk fat oleogel. (Reproduced from [12], with permission from Elsevier); (**i**) CTI, sample: filling creams produced with MG: wax oleogel. (Reproduced from [15], with permission from Elsevier, under the terms of the Creative Commons CC-BY-NC-ND 4.0 license). See Table 20.1 for the meaning of the abbreviations

sample. CLSM has been used to study the crystal network characteristics in oleogels (Fig. 20.1e), but also the interfacial morphology in two-phase and multiphase systems derived from oleogels, such as simple emulsions, Pickering emulsions, bigels (Fig. 20.1f), and oleofoams. Recently, CLSM was used to analyze fluorescence recovery after photobleaching as a method to determine the stability of oleofoams against possible phase separation phenomena [5].

Another advanced imaging technique is atomic force microscopy (AFM), which generates 3D topographical images of samples, with nanometer or even atomic

resolution, by measuring the force interactions between a nanometer-sized probe and the material surface [4]. AFM has been used to study morphological characteristics of crystal and polymeric networks (Fig. 20.1g), geometrical characteristics of crystal surfaces, and the growth mechanism of tubular gelators [6–8].

Confocal Raman microscopy (CRM) combines Raman spectroscopy and confocal microscopy to obtain chemical composition and structural information over a small defined sample area. The identification of compounds present in the sample surface is based on the so-called Raman effect, which is the inelastic scattering of photons produced when monochromatic light interacts with sample molecules [9]. CRM compositional maps have been used to determine the size and porosity of floc crystal networks and fractal dimension in dispersions of micronized fat crystals in oil [10]. The degree of crystallinity and the type and amount of major crystal polymorphs were imaged simultaneously by CRM in porcine adipose tissue, which was used as a model fat system [11]. These methods can also be implemented to study oleogels due to the similarity between the systems. Recently, CRM was applied to visualize the structural distribution of components in oleogels from ethylcellulose and milk fat, as well as to map lipids with different degrees of mobility (liquid vs. solid) within oleogels (Fig. 20.1h) [12].

On the other hand, imaging techniques developed for medical use have been applied to study oleogel-based food products. Nuclear magnetic resonance imaging (MRI) was used to study the distribution of the lipid fraction in oleogel-based sweet bread [13]. On the other hand, X-ray computed tomography imaging (CTI) can be employed to investigate the internal structure of materials in a three-dimensional way. As X-rays pass through the sample, they attenuate according to material density and atomic number, and the intensity of the emerging X-ray is recorded in a series of two-dimensional images, which can be processed to produce cross-sectional images. These multiple images taken from different angles of the sample are then processed using computer software to reconstruct the sample 3D model [3, 14]. This makes CTI an ideal tool for observing the microstructure of porous foods. In the field of oleogels, CRI has been applied to determine morphological parameters of aerated structures of filling creams (Fig. 20.1i) [15]. This method can also be used to examine the structures of other oleogel-based products, including aerated chocolate, bread, cakes, and frozen foods [14].

Images from digital cameras can be suitable to determine macrostructure and macroscopic behavior of specific foods, in which the size of the features is large enough to be captured using low magnifying tools. Processed digital images have been used to determine surface characteristics, porosity, and crumbly grain characteristics in cookies and bakery products, as well as to visualize the consistency of oleogel-based filling creams [13, 16]. Recently, a novel method to determine the oil release kinetics of oleogels during storage was proposed based on automated image analysis [17].

20.2.2 Sample Preparation

Image analysis is a tool that can be applied to any type of images, regardless of sample preparation. For this reason, it is critical that users prepare samples for visualization using an appropriate protocol that minimizes material modification to ensure that the images they obtain are accurate representations of the original sample. Images with artifacts due to improper sample handling will still give results which, however, can be of questionable significance. For example, if a monoglyceride oleogel is imaged using an optical microscope, but the sample is first spread on the glass slide and then a glass coverslip is firmly pressed on top of the sample, the obtained images will likely show a broken and loose monoglyceride network which does not represent the original structure within the oleogel. If these images are analyzed, one can still obtain information, which would lead to improper conclusions. On the other hand, sample treatment is also necessary for certain imaging techniques because of the interference that, for example, oil might cause to the gelator network. In this case, deoiling needs to be applied before imaging. However, the type and amount of solvent, as well as the contact time, and application of fixating agents are factors that greatly influence the outcome [6, 33, 34]. Thus, the deoiling process needs to be optimized to be effective in removing the oil from the oleogel without damaging the network structure.

20.2.3 Commonly Used Software for Image Analysis

To analyze images, they should be in digital form or digitalized after acquisition. Working with digital images allows editing and processing of images before extracting information. Indeed, images need to be transformed to highlight features or objects to be analyzed, increasing their contrast with respect to the background, or masking parts of the image that are not important or that can affect the output of the transformation. More information on image processing is given in the following paragraph. In general, the reader should know at this point that there are two steps in image analysis: processing and information extraction. Dedicated software used in image analysis can perform both operations. However, there are some software developed as image editors that can easily perform the first step but possess limited or no functions to execute the second step. Although there are various software and apps for computers, tablets, and smartphones, here we report the most used and promising ones for image analysis of lipid-based materials and oleogels.

ImageJ and its different versions/evolutions, such as Fiji and ImageJ2, are freeware/open-source software (free of cost) that have been under continuous development since Rasband's pioneering work on the first image analysis software in 1987 [35]. This family of software (https://imagej.net/learn/flavors) has all the necessary basic functions to carry out image analysis for oleogel research. In addition, there are many publicly available plugins developed by the online community and users that

extend the capabilities of these software, such as the FracLac plugin, which allows for the calculation of fractal dimensions of oleogel crystal networks. This family of software has a user-friendly interface that resembles many other software operating in Windows or MacOS.

Image Pro Plus is a licensed software sold by Media Cybernetics that works on 2D images and can be extended to 3D and 4D (time-lapse) images with an additional module. Like ImageJ and its derived software, Image Pro Plus has a user-friendly interface and provide all the necessary functions to perform image analysis for oleogel research.

Photoshop is a licensed software sold by Adobe, which was developed as a raster graphics editor allowing to create and edit images. This software can be used to process and transform images before analysis.

Besides dedicated software for image analysis, programming languages and computing environments like Python (freeware) and MATLAB (from MathWorks, licensed) can also be used for this purpose. Due to the versatility of these languages, it is possible to directly write a code/script that uses in-built functions to process and extract information from images. Although these programming languages are versatile, users need to learn the syntax and find the appropriate command or set of commands to carry out image analysis. To facilitate this operation, libraries and toolboxes are available for both platforms. An example of an image analysis library developed for Python is Scikit-image, where the scientist/programmer community has documented the implementations of common algorithms for image analysis with the aim to facilitate teaching [36]. Another example is the Image Processing Toolbox available for MATLAB, which includes standard algorithms for image analysis and the application of related workflows.

20.2.4 Useful Commands for Image Analysis

In this section, we present the most useful image processing commands that facilitate information extraction, as well as commands that allow to determine basic parameters in image analysis.

Processing is necessary since it optimizes images for extracting information. The main purpose of this step is to visually enhance those features to be analyzed. There are four commands that are mostly used in image processing: *grayscale 8-bit* conversion, *contrast enhancement*, *masking*, and *thresholding*. Besides these four commands, *background subtraction* and *segmentation* are also used in lipid-based materials image processing. The processed images can then be analyzed by *counting/measuring* tools and *Fast Fourier Transform (FFT)*.

Digital images are usually obtained using the RGB color model. This means that each color can be obtained by summing red, green, and blue colors at different intensities and ratios. A digital image is then the result of the overlap of three distinct images having intensities ranging from the darkest to lightest of red, green, and blue colors. Although color can carry information, as seen in CLSM and PLM

micrographs, most of the analysis carried out on oleogel images only requires grayscale images. Therefore, it is common to convert images from RGB to *8-bit grayscale* format. The latter is a compressed image format where the values for each color at each pixel location are averaged (simple average or weighted average, depending on the type of function used), obtaining as a result an image that shows different tonalities of gray. Another commonly used command in image processing is *contrast enhancement*, which helps to identify objects and their features by maximizing their intensity difference with respect to other objects and the background. When illumination is not uniform throughout an image, it is sometimes necessary to *subtract* the *background* before modifying the contrast. In case parts of the image are not of interest, the most convenient action is to create a *mask* to eliminate them. This action creates customizable shapes that are overlapped to the image on specific regions selected by the user. Masks can then be colored to avoid interfering with further image processing. The last widely used command in oleogel image analysis is *thresholding*. This command allows the conversion of 8-bit grayscale images into binary (black and white) images by setting a cutoff value (threshold) of luminosity. Pixels above the threshold are converted to white pixels (usually part of the object of interest ,e.g., crystals in PLM images), while pixels below the threshold are converted to black color, which becomes part of the background. This operation reduces the complexity of images and simplifies the operations during information extraction. Sometimes *thresholding* leads to the opposite result: the objects of interest become black, and the background becomes white. This outcome does not interfere with the analysis as long as the user is aware of the color assigned to the objects of interest. *Thresholding* leads to better results when carried out after all other commands described before. This is because enhancing the difference between the background and the objects of interest improves the thresholding result since this command assumes that images have a bimodal luminosity distribution (light objects + dark background, or vice versa) [37]. If thresholding is carried out on the entire image, it is called *global thresholding*. On the other hand, if thresholding is carried out on each pixel and the cutoff value is based on the neighbor pixels within a restricted area, it is called *local thresholding*. In general, *global thresholding* is more common in oleogel image analysis. It may happen that images show objects that are touching each other, for example, adjacent crystals. If a user applies any of the commands described above, the objects will permanently merge, leading to incorrect results. To avoid this problem, another useful command is *segmentation*, which separates or divides two or more adjacent objects.

After image processing, one can proceed with the extraction of information from images. There are mainly two types of commands used for this scope when analyzing images of oleogel samples: *counting/measuring* and *FFT*. *Counting/measuring* command allows to count, calculate area, dimensions, etc., of objects (e.g., crystals and oil stains) shown in any image. It is also possible to use embedded commands like the *line profile* or *plot profile*, which allow to calculate the intensity of gray value over distance in a line or in a region of interest. In the latter example, the analysis should be carried out on an 8-bit grayscale image. The second type of command,

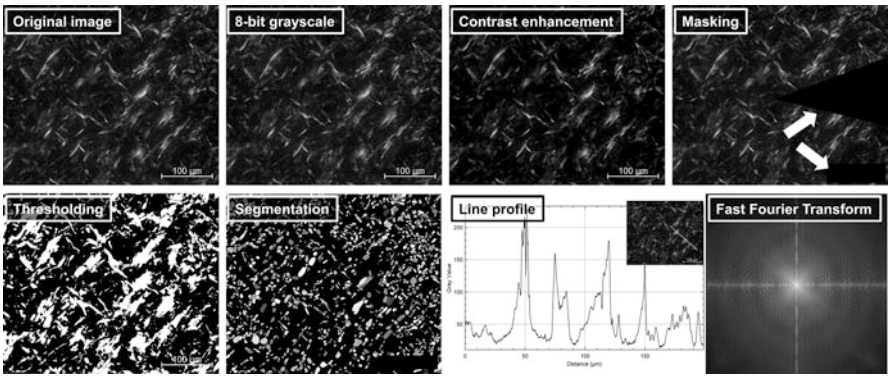

Fig. 20.2 Example of commands used in image analysis. Original image is a polarized light micrograph of a 2.5% w/w sunflower wax oleogel. (Images were processed using Fiji)

FFT, is a mathematical transformation of the image from the spatial to the frequency domain, returning as a result a power spectrum. From the power spectrum, it is possible to obtain information about the sine and cosine components of the signal of the original image in the spatial domain, where each point represents a particular frequency. If repeating patterns are present, they manifest in the power spectrum as spots that propagate in the opposite direction of the repetition in the original pattern. The spots contain information about the repeating distance of the pattern, which is useful in determining, for example, lamellar structures imaged using TEM. It is also worth mentioning that *FFT* can also be used to process images before analyzing them. Indeed, once the image is transformed, it is possible to mask some of the signals in the power spectrum and then apply the *inverse Fourier Transform* to obtain a modified version of the original image (for example, smoothing defects of the original image). An example of all commands applied to an oleogel PLM micrograph described in this section is shown in Fig. 20.2.

As a final note, there may be cases where a series of commands need to be applied to large sets of images. For example, *spatial calibration*, *contrast enhancement*, *masking*, *thresholding*, and *object counting* might have to be executed on hundreds of images. In this case, repeated actions can be automated in image analysis procedures. Depending on the program/programming language used, this can be implemented by recording *macros* (which record the actions performed on the mouse or keyboard and repeat them in sequence) or by embedding *dedicated functions* in the developed code. For more information on other commands available for image analysis, the reader can refer to the help/guide menu of the selected image analysis software as well as to the extensive book of Russ [38] on image analysis of food microstructure.

Practical Recommendations for Image Analysis

- Make sure the images obtained are accurate representations of the original sample by using a sample preparation protocol that minimizes material modification.

- Remember to carry out spatial calibration before processing and analyzing your images. You can use either the scale bar in your image or a reference object of known dimensions. This is the first action that should be performed in the software of your choice after opening or importing the image you want to analyze, before using any of the commands below.

20.3 What Information Can We Extract?

In this section, we describe qualitative and quantitative parameters related to oleogels that can be obtained from image analysis by applying the image processing commands discussed above and other specific commands.

20.3.1 Crystal Shape and Network Morphologies

Oleogels can exhibit different colloidal structures depending on the gelator they are formed from, such as polymeric, crystalline, and self-assembled fibrillar networks [39]. The morphological features of crystalline networks can be defined by the shape, size, and state of agglomeration of crystal particles. These characteristic parameters are usually determined through image analysis of PLM micrographs.

Via PLM observation, the crystal morphologies of lipid gelators, such as MG, waxes, and fatty acids, have been suggested to be needle-like, which are organized into spherulites/rosettes or irregularly shaped clusters [23, 25, 40]. Other gelators, like phytosterols, have shown multiple morphologies with aggregates consisting of fibrous, spherulite, and plate-like crystals [32]. In general, crystalline network morphology can be easily identified using oleogel systems with low gelator concentrations to avoid large-scale agglomerates that could lead to misinterpretation. Furthermore, the use of more than one crystal visualization method is highly recommended [41]. This was evidenced in the study of sunflower wax oleogels, which showed a needle-like crystalline morphology when observed by PLM, while platelets were seen by SEM examination [33, 42]. It was suggested that the needle-like morphology might be a view of a protruding edge of the platelets [33]. PLM micrographs have also been used to evaluate qualitative and quantitative changes in the crystalline network morphology of oleogels from waxes and MG during aging storage [43, 44]. On the other hand, polymeric networks such as ethylcellulose oleogels cannot be visualized under PLM due to the absence of birefringence, requiring alternative imaging techniques with higher resolution like AFM and Cryo-SEM [6].

20.3.2 Crystal Size and Crystal Size Distribution

By measuring the size or length of crystals, it is possible to characterize crystals quantitatively. Using this approach, the effects of composition or processing variables on crystal structure can be systematically and accurately identified. When oleogels are composed of uniform-shaped crystals, the average crystal size, or the average crystal length in the case of needle-like particles, and the standard deviation are suitable parameters to characterize the crystalline network. A PLM, CLSM, and RM micrograph can show dozens of crystals that can be measured using a measuring tool from suitable software (e.g., ImageJ) with a previously calibrated scale. Crystal length measurements should be made on individual crystals, even in the case of cluster formations [44]. However, a particle size distribution analysis is most appropriate when oleogels are composed of crystals of irregular sizes. This approach involves using the total of size measurements (recommended value >100) to generate a frequency histogram; for example, using the Histogram tool from the Analysis ToolPak of Excel (Microsoft Office). The size distribution is then described in terms of D_{50}, the median, and Span, the width. Span is calculated as $(D_{90} - D_{10})/D_{50}$, with D_{10}, $D_{50,}$ and D_{90} being the particle size where 10, 50, and 90% of the population, respectively, lies below these values [23].

20.3.3 Pore Area Fraction and Crystalline Area

The determination of the area unoccupied by crystals, known as the pore area fraction (PAF), is a simple and useful method for characterizing the crystalline microstructure of oleogels. To calculate PAF (%), images are converted to *8-bit type* and processed using *global auto thresholding* to transform the original image into the form of white objects on a black background. The area (%) of white pixels in each image is representative of solid crystalline material, quantifiable by processing software. Therefore, the PAF can be calculated as the remaining area [23, 45]. In the case of images that cannot be processed by the automatic thresholding tool due to the color similarity between the crystals and the oil, a command that segments the color space present in the images can be used to divide the areas corresponding to crystals and oil. For example, the *Color Inspector 3D plugin* from ImageJ, which allows the generation of color histograms by segmentation of the color space presented in the images. With this, different colors of the image are identified—using RGB color model—and their absolute and relative frequencies are listed. To reduce the number of segments, images can be converted into *32-bit gray scale* images, resulting in histograms of 32 colors. From the histogram, the percentage of area corresponding to each segment is obtained. By visual inspection, each segment can be classified as either crystalline or oil structure, and then the areas corresponding to each type are summed up [23].

Previous work has pointed out the importance of imaging techniques and sample preparation in obtaining representative PAF values. When PLM, CLSM, and RM images of MG oleogels produced in a rheometer were used to determine PAF, different results were obtained among techniques [23]. The authors attributed this behavior to the fact that PLM and CLSM images were acquired from oleogel samples that were removed from the rheometer plate and placed between a slide and a coverslip. This procedure would keep the crystal structure intact, but probably not the oil distribution, which would be affected by the pressure exerted on the coverslip to achieve a thin enough sample for microscopy. In contrast, the RM images were captured directly *in situ* during oleogel formation, without subsequent manipulation, resulting in more accurate PAF results. Similarly, special care should be taken when samples are prepared by depositing a drop of molten oleogel on a microscope slide and covering it with a coverslip. A standardized procedure should be followed to avoid introducing variations between samples through manipulation.

20.3.4 The Box-Counting Fractal Dimension of Crystalline Area

The fractal dimension (D) is an index of space-filling properties used to describe surfaces whose irregular nature cannot be explained by traditional geometric terms. This parameter can be used as an indicator of the crystal mass distribution in oleogel networks. The higher D, the more homogeneously distributed mass and/or uniformly filled space [45]. Different computing methods can be applied to obtain D, with *box counting* (D_{bc}) being the most widely used. For this purpose, micrographs of oleogels are converted into *8-bit binary* images. Using the tool for D_{bc} calculation of an image analysis software, this parameter is determined automatically. In the case of ImageJ, D_{bc} can be determined by the *FracLac plugin* (option: BC). For more information on *FracLac plugin*, the reader can refer to its online manual (https://imagej.net/ij/plugins/fraclac/FLHelp/BoxCountingOptions.htm).

The D_{bc} algorithm consists of systematically laying a series of grids of decreasing length size r (the boxes), being $N(r)$ the number of boxes required to cover the mass area present in the image. For each successive length (scale), the N value is recorded. Then D_{bc} is calculated by evaluating how N varies with decreasing r [46]:

$$D_{bc} = \lim_{r \to 0} \frac{\log\ N\ (r)}{\log\ (1/r)} \tag{20.1}$$

In practice, D_{bc} is calculated as the slope of the line obtained by plotting log $(1/r)$ vs. log $(N\ (r))$. On the other hand, if three-dimensional gel features are to be represented, an additional dimension must be added to obtain D ($D = D_{bc} + 1$) [47].

D_{bc} has been used as a microstructural parameter to analyze the effects of the type of gelator and its concentration and cooling temperature during oleogel production

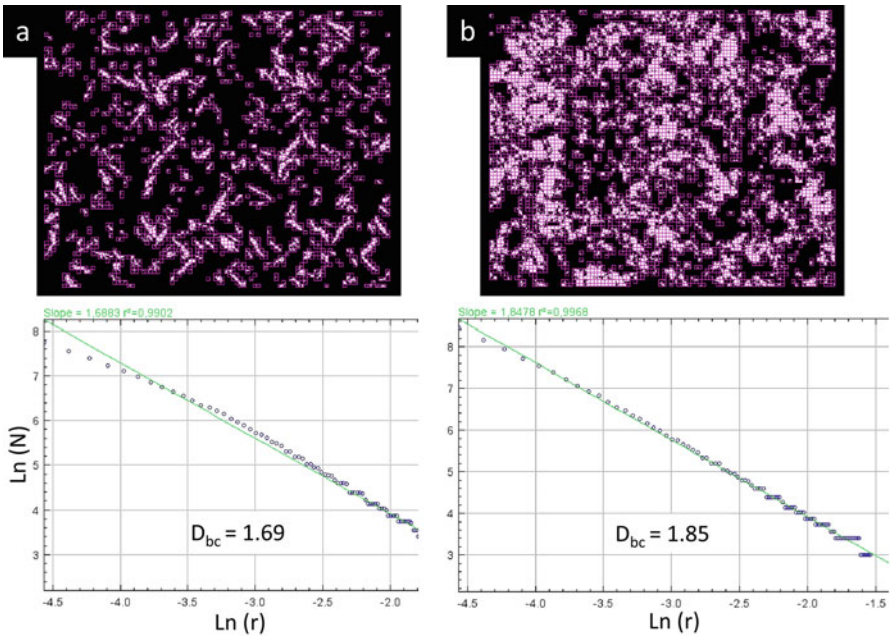

Fig. 20.3 PLM images of oleogel-based emulsions from (**a**) commercial and (**b**) recovered sunflower waxes processed by *FracLac* using box-counting analysis. The graphs show the linear regression generated by the program. The parameters in *FracLac* were set as follows: Image type = ¨use binary¨ and ¨locked black background¨ (it means that measurement is made over white part of figure, which correspond to crystalline area), number of positions for grids G = 1, maximum sizes = 45% of the total image area. Grids are indicated in violet color. Wax oleogels were produced at the same wax concentration (2% w/w). (Images adapted from [48], with permission from Wiley)

[23, 45, 48]. For example, oleogel-based emulsions formulated with recovered sunflower waxes showed higher D_{bc} values than those formulated with commercial ones (Fig. 20.3), which was consistent with a network formed by smaller crystals [42, 48]. Furthermore, the relationship between D_{bc} and solid lipid content has been studied in systems composed of MG or saturated triacylglycerols (tripalmitin and tristearin) and liquid triacylglycerols (medium chain triacylglycerols) [24]. The authors related the minimum solid lipid content able to reach a plateau value of D_{bc} to the network-forming ability and the type of crystals developed (e.g., platelet-like crystals and spherulites).

20.3.5 Kinetics of Crystallization

Image analysis can be used to determine the type of nucleation and dimensionality of crystal growth, both critical factors that determine microstructure characteristics and,

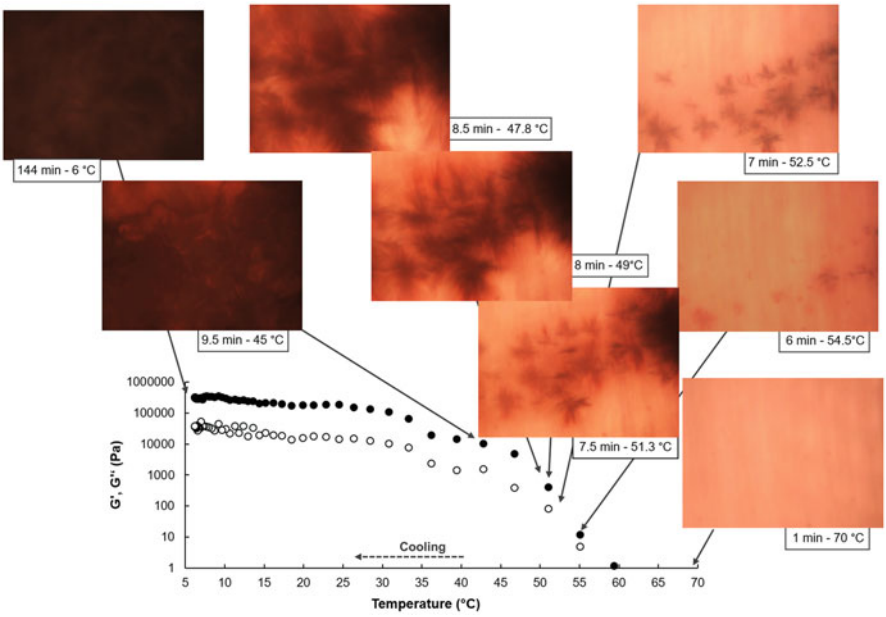

Fig. 20.4 Rheo-microscope images acquired during the formation process of a monoglyceride oleogel in a sweep temperature test (G′ [●] and G″ [○]). All acquired images were processed as indicated in Sect. 20.3.5 to model the kinetic of crystallization. (Adapted from [23], with permission from Elsevier)

consequently, the macroscopic behavior of oleogels. For this purpose, micrographs of the sample are taken during the cooling process. At first, only a homogeneous phase corresponding to the molten oleogel can be imaged. In the following stages, as the temperature decreases, the appearance of the first crystal nuclei and the subsequent crystal growth and branching is recorded (Fig. 20.4) [23]. After that, the images are processed to obtain a parameter (Y_s) that represents the crystal phase volume formed until a given time [49].

Non-isothermal crystallization kinetics of crystal particles can be appropriately described by a modified Avrami model, which is an adaptation of the original equation from isothermal cooling to non-isothermal cooling conditions [49, 50]:

$$\frac{Y_s}{Y_{max}} = 1 - e^{-k_{app}(t-t_0)^n} \tag{20.2}$$

where Y_{max} is the maximal crystal phase volume, k_{app} is the apparent crystallization rate constant, t is the time, t_0 is the induction time, and n is the Avrami index, which indicates both the nucleation mode (sporadic or instantaneous) and the dimensionality of growth (1D, 2D, 3D) [49]. k_{app}, t_0, and n parameters can be obtained by nonlinear curve fitting of experimental data of Y_s/Y_{max} versus t.

This approach was applied by Rogers and Marangoni [50] to analyze the nucleation and fiber growth kinetics of 12-hydroxystearic acid in canola oil. The authors used brightfield images acquired during cooling to first identify the type of nucleation process and then to determine the crystal fiber growth rate using Eq. 20.2, with Y_s being the average fiber length measured by ImageJ. Similarly, Avrami indices were accurately calculated from data extracted from PLM micrographs during crystallization of 12-hydroxystearic acid, stearic acid, and trihydroxystearin, with Y_s determined as crystal length, platelet area, and sphere area, respectively (Ho Lam & Rogers, 2011). More recently, Palla et al. [23] studied the crystallization of MG oleogels at different cooling profiles using RM images acquired during temperature sweep rheological tests and processed using the Color Inspector 3D plugin of ImageJ (see Sect. 20.3.3). The authors followed the crystallization process by quantifying the amount of crystalline solid material over time, that is, the percentage of crystal area in each RM image. Thus, Y_s/Y_{max} was defined as %crystal area (t)/%maximal crystal area. An Avrami index close to 2 was found for all cooling profiles tested, which was associated with an MG crystallization characterized by sporadic nucleation and crystal growth in needle-like form (1D). Interestingly, the authors also found that the RM images could be used to identify the temperature range at which the MG crystals formed, thereby determining a more restricted time domain in which Eq. 20.2 could also be used to calculate the Avrami index but based on the evolution of the complex viscosity.

20.3.6 Polymorphism and Lamellar Dimension

Oleogels obtained by structuring oil with self-assembly crystalline gelators can contain repeating stacked lamellar structures at nanoscale. To the best of our knowledge, these nanostructures have been observed in TEM images of oleogels derived from waxes, stearic acid, stearyl alcohol, and MG [18, 27, 28], where they resembled those present in crystalline nanoplatelets composed of saturated triacylglycerols [51]. In this case, image analysis can be used to determine the dimensions of these lamellar structures. For example, by applying FFT to selected areas of TEM images where the lamellar structures can be observed, it is possible to obtain the power spectrum of the image and calculate interplanar distances. This method was described by Sánchez-Becerril et al. [27] on candelilla wax-based oleogels, where the authors determined the presence of CW β′ polymorphic form, further confirmed using XRD. Through the power spectrum of TEM images, lamellar dimensions of triacylglycerols in crystal nanoplatelets were also determined [52]. In general, characteristic dimensions of any repeating patterns in lipid-based materials can be calculated by applying FFT to TEM images [53], complementing the image analysis with XRD analysis.

20.3.7 Oil Mobility

Oil mobility can be determined by calculating the relaxation time of protons associated with lipids by using nuclear magnetic resonance (NMR) [54, 55]. However, to determine the location of mobile protons in a matrix/sample, it is necessary to use magnetic resonance imaging (MRI). In this case, the grayscale images obtained show bright areas that can be attributed to mobile protons belonging to oil or water. In a work by Calligaris et al. [13], oil mobility in sweet breads containing oleogels, other fat replacers, and palm oil and sunflower oil (controls) was calculated on magnetic resonance images using image analysis. The authors first demonstrated that bright areas on images could be attributed to oil (by suppressing the signal generated by lipids using a dedicated Spin-Echo mode). They then acquired images of sweet bread slices and calculated the total area of bright pixels (above a set threshold) with respect to the total area of the slice, concluding that lipid structuring plays a critical role on lipid distribution and mobility in their samples.

20.3.8 Oil Release

An important parameter for evaluating oleogel structure and stability is oil release. The oil contained in oleogels is mobile and can migrate out from the oleogel structure. This phenomenon, known as oil release or oil leakage, can occur at different magnitudes and times depending on the trapping ability of the gelator network and possible molecular rearrangements of gelators during storage [55–57]. Recently, Valoppi et al. [17] developed a novel automated method to determine oil release from oleogels using image analysis. The authors designed an inexpensive system featuring a tripod with a circular opening, filter paper, a digital camera, and a computer. Oleogels placed on a filter paper produce an oil stain that radiates out from the sample. By acquiring images from the bottom of the tripod over time, it is possible to obtain information on the evolution of the area of the oil stain and calculate the oil release kinetics. The authors automated image acquisition, processing and analysis using custom-made scripts for ImageJ. The result of the analysis is shown in Fig. 20.5. This method has also been used to evaluate the oil release of oleogels modified using ultrasonic standing waves [58].

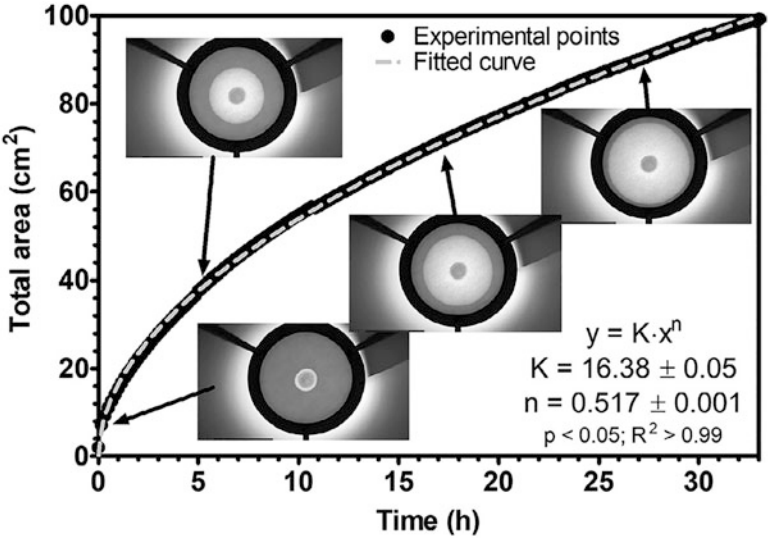

Fig. 20.5 Evolution over time of an oil stain area formed by the radial diffusion of oil from an oleogel placed on a filter paper. Data were generated using a set of 200 images captured over 33 h. Images reported in the figure show the evolution of the oil stain (annular white area) at selected time points. Fitted curve and regression analysis results are also shown. (Reproduced from [17], under the terms of the Creative Commons CC-BY license)

20.4 The (Potential) Use of Machine Learning in Image Analysis of Oleogels

Machine learning (ML) is a branch of artificial intelligence (AI), in which a computer learns from given datasets without being directly programmed, and builds mathematical models that are later used to perform specific tasks. Computers are usually trained on large datasets (labeled in case of supervised ML, or unlabeled in case of unsupervised ML) that are used to build and refine the models developed. Since ML is an iterative process, the models developed during learning are constantly improved based on new imputed datasets. ML is a versatile technique that can handle large and complex datasets, such as images, and it has been applied in image analysis of various materials [59]. Indeed, images can be considered as matrices of numbers where each pixel is identified by coordinate values (e.g., x and y in 2D images) associated with color values expressed using the RGB color model (as discussed in Sect. 20.2.4). Therefore, images can be treated as mathematical functions and be used as datasets for building models through ML. In this case, images can be analyzed using computational methods like digital image processing (DIP) by employing programming languages like Python. However, it is worth mentioning that usually the images acquired by the techniques described above (Sect. 20.2.1) represent small datasets for ML training. To overcome this problem, some solutions are available. In particular, dataset augmentation, which includes

zooming, flipping, and contrast change on the same image (one image can be used multiple times), or transfer learning, where a certain problem is solved using a pre-trained ML on similar datasets, can be used to enlarge datasets for ML [59]. Although ML is a powerful tool for image analysis, to the best of our knowledge, there are no articles mentioning the use of this technique or other forms of AI for the analysis of oleogel images. However, due to the continuing advances in ML application and oleogel area, we might expect further research in this field.

20.5 Conclusions

Image analysis is a powerful tool to investigate the nano, micro, and macro characteristics of oleogels and oleogel-based systems. To obtain reliable results, images need to be representative of the sample and it is vital to avoid artifacts caused by improper sample preparation. Moreover, using more than one visualization technique is highly recommended. Throughout this chapter, the main techniques available for acquiring oleogel images have been presented, as well as the most used software and commands for image processing and analysis. The emergence of advanced microscopy techniques and the development of powerful software have made it possible to extract a wide variety of information from oleogel images. Image analysis finds a wide field of application in oleogels formed by a crystalline network, in which not only qualitative features can be determined but also quantitative parameters such as crystal size, porosity and network crystalline area, fractal dimension, kinetics of crystallization, and even the type of polymorphic form present and the lamellar structure. On the other hand, macroscopic images can be especially useful to evaluate the oil stability behavior of oleogels, as well as the macroscopic characteristics of food products made with oleogels. It is expected that in the coming years image analysis will be applied to the study of more complex oleogel-based systems, and that novel tools such as machine learning and other forms of artificial intelligence may also bring new methodologies to the study of oleogels.

Acknowledgments Camila Palla acknowledges the Consejo Nacional de Investigaciones Científicas y Técnicas (CONICET) of Argentina. Fabio Valoppi acknowledges the European Union's Horizon 2020 research and innovation program funding under the Marie Skłodowska-Curie grant agreement No. 836071.

References

1. Shi X, Zhao S, Wang F, Jiang Q, Zhan C, Li R, Zhang R (2021) Optical visualization and imaging of nanomaterials. Nanoscale Adv 3:889–903. https://doi.org/10.1039/d0na00945h
2. Ebnesajjad S (2011) Surface and material characterization techniques. In: Ebnesajjad S (ed) Handbook of adhesives and surface preparation. William Andrew Publishing, Norwich, pp 31–48
3. Verboven P, Defraeye T, Nicolai B (2018) Measurement and visualization of food microstructure. In: Devahastin S (ed) Food microstructure and its relationship with quality and stability. Woodhead Publishing, Sawston, pp 3–28
4. Metilli L, Francis M, Povey M, Lazidis A, Marty-Terrade S, Ray J, Simone E (2020) Latest advances in imaging techniques for characterizing soft, multiphasic food materials. Adv Colloid Interface Sci 279:102154. https://doi.org/10.1016/j.cis.2020.102154
5. Andriotis EG, Monou PK, Komis G, Bouropoulos N, Ritzoulis C, Delis G, Kiosis E, Arsenos G, Fatouros DG (2022) Effect of glyceryl monoolein addition on the foaming properties and stability of whipped oleogels. Gels 8:705. https://doi.org/10.3390/gels8110705
6. Zetzl AK, Gravelle AJ, Kurylowicz M, Dutcher J, Barbut S, Marangoni AG (2014) Microstructure of ethylcellulose oleogels and its relationship to mechanical properties. Food Struct 2: 27–40. https://doi.org/10.1016/j.foostr.2014.07.002
7. Matheson AB, Koutsos V, Dalkas G, Euston S, Clegg P (2017) Microstructure of beta-sitosterol: Gamma-oryzanol edible organogels. Langmuir 33:4537–4542. https://doi.org/10.1021/acs.langmuir.7b00040
8. Lupi FR, De Santo MP, Ciuchi F, Baldino N, Gabriele D (2018) The role of edible oils in low molecular weight organogels rheology and structure. Food Res Int 111:399–407. https://doi.org/10.1016/j.foodres.2018.05.050
9. Hassen SM, Mofdal MEE (2018) Using Raman spectroscopy to identify unknown materials. Int J Appl Phys 5:29–32. https://doi.org/10.14445/23500301/IJAP-V5I3P105
10. Martens KJA, van Dalen G, Heussen PCM, Voda MA, Nikolaeva T, van Duynhoven JPM (2018) Quantitative structural analysis of fat crystal networks by means of raman confocal imaging. J Am Oil Chem Soc 95:259–265. https://doi.org/10.1002/aocs.12035
11. Motoyama M, Ando M, Sasaki K, Nakajima I, Chikuni K, Aikawa K, Hamaguchi HO (2016) Simultaneous imaging of fat crystallinity and crystal polymorphic types by raman microspectroscopy. Food Chem 196:411–417. https://doi.org/10.1016/j.foodchem.2015.09.043
12. Gómez-Mascaraque LG, Tran C, O'Callaghan T, Hogan SA (2021) Use of confocal Raman imaging to understand the microstructure of anhydrous milk fat-based oleogels. Food Struct 30: 100228. https://doi.org/10.1016/j.foostr.2021.100228
13. Calligaris S, Manzocco L, Valoppi F, Nicoli MC (2013) Effect of palm oil replacement with monoglyceride organogel and hydrogel on sweet bread properties. Food Res Int 51:596–602. https://doi.org/10.1016/j.foodres.2013.01.007
14. Cornish A (2019) X-ray ct imaging of food. Food Sci Technol 33:30–33. https://doi.org/10.1002/fsat.3303_8.x
15. Kim M, Hwang H-S, Jeong S, Lee S (2022) Utilization of oleogels with binary oleogelator blends for filling creams low in saturated fat. LWT- Food Sci Technol 155:112972. https://doi.org/10.1016/j.lwt.2021.112972
16. Giacomozzi AS, Carrin ME, Palla CA (2018) Muffins elaborated with optimized monoglycerides oleogels: from solid fat replacer obtention to product quality evaluation. J Food Sci 83: 1505–1515. https://doi.org/10.1111/1750-3841.14174
17. Valoppi F, Lassila P, Salmi A, Haeggström E (2021) Automated image analysis method for oil-release test of lipid-based materials. MethodsX 8:101447. https://doi.org/10.1016/j.mex.2021.101447
18. Rosen-Kligvasser J, Davidovich-Pinhas M (2021) The role of hydrogen bonds in tag derivative-based oleogel structure and properties. Food Chem 334:127585. https://doi.org/10.1016/j.foodchem.2020.127585

19. Wettlaufer T, Hetzer B, Flöter E (2021) Characterization of oleogels based on waxes and their hydrolyzates. Eur J Lipid Sci Technol 123:2000345. https://doi.org/10.1002/ejlt.202000345
20. Brykczynski H, Hetzer B, Flöter E (2022) An attempt to relate oleogel properties to wax ester chemical structures. Gels 8:579. https://doi.org/10.3390/gels8090579
21. Saha S, Saint-Michel B, Leynes V, Binks BP, Garbin V (2020) Stability of bubbles in wax-based oleofoams: decoupling the effects of bulk oleogel rheology and interfacial rheology. Rheol Acta 59:255–266. https://doi.org/10.1007/s00397-020-01192-x
22. Blake AI, Marangoni AG (2015) The use of cooling rate to engineer the microstructure and oil binding capacity of wax crystal networks. Food Biophys 10:456–465. https://doi.org/10.1007/s11483-015-9409-0
23. Palla C, de Vicente J, Carrin ME, Galvez Ruiz MJ (2019) Effects of cooling temperature profiles on the monoglycerides oleogel properties: a rheo-microscopy study. Food Res Int 125:108613. https://doi.org/10.1016/j.foodres.2019.108613
24. Calligaris S, Valoppi F, Barba L, Anese M, Nicoli MC (2018) B-carotene degradation kinetics as affected by fat crystal network and solid/liquid ratio. Food Res Int 105:599–604. https://doi.org/10.1016/j.foodres.2017.11.062
25. Lupi FR, Greco V, Baldino N, de Cindio B, Fischer P, Gabriele D (2016) The effects of intermolecular interactions on the physical properties of organogels in edible oils. J Colloid Interface Sci 483:154–164. https://doi.org/10.1016/j.jcis.2016.08.009
26. Okuro PK, Tavernier I, Bin Sintang MD, Skirtach AG, Vicente AA, Dewettinck K, Cunha RL (2018) Synergistic interactions between lecithin and fruit wax in oleogel formation. Food Funct 9:1755–1767. https://doi.org/10.1039/c7fo01775h
27. Sánchez-Becerril M, Marangoni AG, Perea-Flores MJ, Cayetano-Castro N, Martínez-Gutiérrez H, Andraca-Adame JA, Pérez-Martínez JD (2018) Characterization of the micro and nanostructure of the candelilla wax organogels crystal networks. Food Struct 16:1–7. https://doi.org/10.1016/j.foostr.2018.02.001
28. Golodnizky D, Rosen-Kligvasser J, Davidovich-Pinhas M (2021) The role of the polar head group and aliphatic tail in the self-assembly of low molecular weight molecules in oil. Food Struct-Neth 30:100240. https://doi.org/10.1016/j.foostr.2021.100240
29. Qi WH, Li T, Zhang ZS, Wu T (2021) Preparation and characterization of oleogel-in-water pickering emulsions stabilized by cellulose nanocrystals. Food Hydrocoll 110:106206. https://doi.org/10.1016/j.foodhyd.2020.106206
30. Cho K, Tarté R, Acevedo NC (2023) Development and characterization of the freeze-thaw and oxidative stability of edible rice bran wax-gelatin biphasic gels. LWT- Food Sci Technol 174:114330. https://doi.org/10.1016/j.lwt.2022.114330
31. Jeong S, Lee S, Oh I (2021) Development of antioxidant-fortified oleogel and its application as a solid fat replacer to muffin. Foods 10:3059. https://doi.org/10.3390/foods10123059
32. Bin Sintang MD, Rimaux T, Van de Walle D, Dewettinck K, Patel AR (2016) Oil structuring properties of monoglycerides and phytosterols mixtures. Eur J Lipid Sci Technol. https://doi.org/10.1002/ejlt.201500517
33. Blake AI, Marangoni AG (2015) Plant wax crystals display platelet-like morphology. Food Struct 3:30–34. https://doi.org/10.1016/j.foostr.2015.01.001
34. Rogers MA, Smith AK, Wright AJ, Marangoni AG (2007) A novel cryo-sem technique for imaging vegetable oil based organogels. J Am Oil Chem Soc 84:899–906. https://doi.org/10.1007/s11746-007-1122-9
35. Schneider CA, Rasband WS, Eliceiri KW (2012) Nih image to imagej: 25 years of image analysis. Nat Methods 9:671–675. https://doi.org/10.1038/nmeth.2089
36. van der Walt S, Schonberger JL, Nunez-Iglesias J, Boulogne F, Warner JD, Yager N, Gouillart E, Yu T, scikit-image, c. (2014) Scikit-image: image processing in python. PeerJ 2:e453. https://doi.org/10.7717/peerj.453
37. Bankman IN (2009) Handbook of medical image processing and analysis. Elsevier, Amsterdam
38. Russ JC (2005) Image analysis of food microstructure. CRC Press, Boca Raton

39. Co ED, Marangoni AG (2018) Chapter 1 - Oleogels: an introduction. In: Marangoni AG, Garti N (eds) Edible oleogels, 2nd edn. AOCS Press, Urbana, pp 1–29
40. Sagiri SS, Singh VK, Pal K, Banerjee I, Basak P (2015) Stearic acid based oleogels: a study on the molecular, thermal and mechanical properties. Mater Sci Eng C 48:688–699. https://doi.org/10.1016/j.msec.2014.12.018
41. Flöter E, Wettlaufer T, Conty V, Scharfe M (2021) Oleogels—their applicability and methods of characterization. Molecules 26:1673. https://doi.org/10.3390/molecules26061673
42. Merchán Sandoval J, Carelli A, Palla C, Baumler E (2020) Preparation and characterization of oleogel emulsions: a comparative study between the use of recovered and commercial sunflower waxes as structuring agent. J Food Sci 85:2866–2878. https://doi.org/10.1111/1750-3841.15361
43. Doan CD, Tavernier I, Bin Sintang MD, Danthine S, Van de Walle D, Rimaux T, Dewettinck K (2017) Crystallization and gelation behavior of low- and high melting waxes in rice bran oil: a case-study on berry wax and sunflower wax. Food Biophys 12:97–108. https://doi.org/10.1007/s11483-016-9467-y
44. Giacomozzi AS, Carrin ME, Palla CA (2021) Storage stability of oleogels made from monoglycerides and high oleic sunflower oil. Food Biophys 16:306–316. https://doi.org/10.1007/s11483-020-09661-9
45. Blake AI, Marangoni AG (2015) The effect of shear on the microstructure and oil binding capacity of wax crystal networks. Food Biophys 10:403–415. https://doi.org/10.1007/s11483-015-9398-z
46. Torre IG, Heck RJ, Tarquis AM (2020) Multifrac: an imagej plugin for multiscale characterization of 2d and 3d stack images. SoftwareX 12:100574. https://doi.org/10.1016/j.softx.2020.100574
47. Dàvila E, Parés D (2007) Structure of heat-induced plasma protein gels studied by fractal and lacunarity analysis. Food Hydrocoll 21:147–153. https://doi.org/10.1016/j.foodhyd.2006.02.004
48. Merchán Sandoval J, Carelli A, Baümler E, Palla CA (2020) Relationship between microstructure, rheological behavior and kinetic stability of oleogel emulsions produced with recovered and commercial sunflower waxes. In: International conference of production research (ICPR), Bahía Blanca, Argentina
49. Ho Lam RS, Rogers MA (2011) Experimental validation of the modified Avrami model for non-isothermal crystallization conditions. CrstEngComm 13:866–875. https://doi.org/10.1039/c0ce00523a
50. Rogers MA, Marangoni AG (2008) Non-isothermal nucleation and crystallization of 12-hydroxystearic acid in vegetable oils. Cryst Growth Des 8:4596–4601. https://doi.org/10.1021/cg8008927
51. Acevedo NC, Marangoni AG (2010) Characterization of the nanoscale in triacylglycerol crystal networks. Cryst Growth Des 10:3327–3333. https://doi.org/10.1021/cg100468e
52. Ramel PR, Co ED, Acevedo NC, Marangoni AG (2016) Structure and functionality of nanostructured triacylglycerol crystal networks. Prog Lipid Res 64:231–242. https://doi.org/10.1016/j.plipres.2016.09.004
53. Bunjes H, Steiniger F, Richter W (2007) Visualizing the structure of triglyceride nanoparticles in different crystal modifications. Langmuir 23:4005–4011. https://doi.org/10.1021/la062904p
54. Gravelle AJ, Davidovich-Pinhas M, Zetzl AK, Barbut S, Marangoni AG (2016) Influence of solvent quality on the mechanical strength of ethylcellulose oleogels. Carbohydr Polym 135:169–179. https://doi.org/10.1016/j.carbpol.2015.08.050
55. Rogers MA, Wright AJ, Marangoni AG (2008) Engineering the oil binding capacity and crystallinity of self-assembled fibrillar networks of 12-hydroxystearic acid in edible oils. Soft Matter 4:1483–1490. https://doi.org/10.1039/b803299h
56. Valoppi F, Calligaris S, Marangoni AG (2017) Structure and physical properties of oleogels containing peanut oil and saturated fatty alcohols. Eur J Lipid Sci Technol 119:1600252. https://doi.org/10.1002/ejlt.201600252

57. Blake AI, Co ED, Marangoni AG (2014) Structure and physical properties of plant wax crystal networks and their relationship to oil binding capacity. J Am Oil Chem Soc 91:885–903. https://doi.org/10.1007/s11746-014-2435-0
58. Lassila P, Valoppi F, Tommiska O, Hyvönen J, Holmström A, Hietala S, Salmi A, Haeggström E (2022) Practical scale modification of oleogels by ultrasonic standing waves. Ultrason Sonochem 85:105970. https://doi.org/10.1016/j.ultsonch.2022.105970
59. Pratap A, Sardana N (2022) Machine learning-based image processing in materials science and engineering: a review. Mater Today Proc 62:7341–7347. https://doi.org/10.1016/j.matpr.2022.01.200